Proceedings of the ASME 2024 Heat Transfer Summer Conference
HT2024
July 15-17, 2024, Anaheim, California

HT2024-130166

ADVANCEMENT IN LITHIUM-ION BATTERY PACK THERMAL MODELING BASED ON ELECTROCHEMICAL PRINCIPLES

Patryck Ferreira
Texas Tech University
Lubbock, TX

Shu-Xia Tang*
Texas Tech University
Lubbock, TX

ABSTRACT

This study introduces an advanced thermal model for lithium-ion battery packs, examining cell and module-level heat dynamics. Heat within cells originates from complex electrochemical reactions described by Fick's second law. The Single Particle Model (SPM) utilizes two Partial Differential Equations (PDEs) to analyze electrode dynamics, considering electric power generation via Ohm's law and subsequent heat generation from Joule's effect. Conduction interactions within cells and the battery casing are assessed using a thermal resistance model. Convective heat within the liquid electrolyte is also considered in the cell heat analysis. This cumulative heat is averaged per cell within a module to determine total module heat. A transient heat equation, employing PDEs, analyzes internal module temperatures, incorporating the heat exchange system as boundary conditions, creating a system of PDEs for each module. This approach, distinct from computational fluid dynamics studies, focuses on detailed cell-level modeling using PDEs, extending to module-level heat analysis with boundary conditions. The study's novelty lies in its method of employing multiple PDEs to model module temperature within battery packs, improving accuracy and safety assessment.

Keywords: Electrochemical-Thermal Model, Lithium-ion Battery, Battery Pack, Single Particle Model, Transient Heat Equation.

NOMENCLATURE

A_{cell}	Area where the electrolyte is applied	[m^2]
$A_{\text{conv,ex},i}$	Internal area of the heat exchange system	[m^2]
c_p	Heat capacity	[$\text{J kg}^{-1}\,\text{K}^{-1}$]
$c_s^{\pm}$	Solid phase concentration	[mol m^{-3}]
C_{max}	Maximum concentration	[mol m^{-3}]
$D_s^{\pm}$	Diffusion of the solid phase	[$\text{m}^2\,\text{s}^{-1}$]
F	Faraday constant	[C mol^{-1}]
h_{cell}	Electrolyte convective heat transfer	[$\text{W m}^{-2}\,\text{K}$]
$h_{\text{conv,ex},i}$	Working fluid convective heat transfer	[$\text{W m}^{-2}\,\text{K}$]
I	Current applied to the battery	[A]
$j^{\pm}$	Molar flux	[$\text{mol m}^{-2}\,\text{s}^{-1}$]
k	Thermal conductivity	[$\text{W m}^{-1}\,\text{K}^{-1}$]
k_{cell}	Thermal conductivity of each part	[$\text{W m}^{-1}\,\text{K}^{-1}$]
k_s	Thermal conductivity	[$\text{W m}^{-1}\,\text{K}^{-1}$]
L_{cell}	Length of each internal part of the battery	[m]
L_x	Length of the module unit in the x-direction	[m]
$L_{y,i}$	Length of the module unit in the y-direction	[m]
$L^{\pm}$	Length of the positive or negative electrode	[m]
$q_{\text{cond,ex},i}$	Conductive heat in each module	[W]
$q_{\text{cond,cell}}$	Conductive heat transfer in the cell	[W]
$q_{\text{conv,ex},i}$	Convective heat in the heat exchange system	[W]
$q_{\text{conv,cell}}$	Convective heat in the cell	[W]
Q_{cell}	Heat generated in each cell	[W]
Q_{module}	Heat generated within the battery module	[W m^{-3}]
r_1	Internal radius of the cell	[m]
r_2	External radius of the cell	[m]
R_{i}	Thermal resistance	[K W^{-1}]
$R^{\pm}$	Particle radius	[m]
$R_f^{\pm}$	Resistance	[Ω]
ρ	Density	[kg m^{-3}]
S_{cell}	Electrochemical heat	[W]
T_{fluid}	Temperature of the working fluid	[°C]
T_{i}	Temperature in each module	[°C]
$U^{\pm}$	Equilibrium potential	[V]
V	Voltage	[V]
$\eta^{\pm}$	Overpotential	[V]
$^{+}$	Positive electrode	
$^{-}$	Negative electrode	

1. INTRODUCTION

Lithium-ion batteries find applications ranging from watches to electric vehicles due to their versatility. Electric vehicles, in particular, demand significant energy and power [1]. Combinations of lithium-ion cells, arranged in series, parallel, or a combination of both, form modules, collectively constituting a battery pack to meet these demands. This integration not only serves the energy requirements of electric vehicles but also holds

*Corresponding author: Shu-Xia Tang

immense potential in reducing gas emissions and environmental pollution [2].

Managing battery packs poses challenges, particularly in maintaining the individual cells' state of health after prolonged use, as variations in electrical and thermal interactions among cells often result in non-uniform states of health [3]. Charging all cells to maximum capacity becomes unfeasible, as some cells could exceed their maximum voltage threshold, resulting in thermal instability [4]. This instability may lead to overheating, triggering a chain reaction known as thermal runaway. In large battery packs, thermal runaway can cause widespread damage [5].

Safety measures often rely on over-designing battery packs, incorporating packaging and passive cooling techniques tailored for worst-case scenarios [6]. For instance, Tesla's Model S battery pack employs a heat exchange system to remove heat from all modules in the pack, utilizing a mixture of water and glycol as a working fluid [7]. This system effectively manages thermal dynamics in each module, significantly enhancing the pack's safety standards.

To address these safety concerns, mitigating the risks linked to thermal instability and runaway in lithium-ion batteries remains a crucial focus in advancing battery pack technology. This study represents a preliminary step in thermal modeling by developing a comprehensive approach to determining temperatures within battery packs. The model effectively considers the thermal power generated in each cell and extends its applicability to the entire pack.

The contributions of this study are summarized as follows:

- Employing the Single Particle Model (SPM), this study determines the heat generation within each battery due to electrochemical reactions. This approach contrasts with reference [8], which uses the equivalent circuit model to assess the generated heat.

- Recognizing that heat exchange system plays a pivotal role in dissipating the battery pack's heat, this study integrates the heat exchange system as a boundary condition for each module. This approach, unlike studies such as [9], which estimate temperatures in the cooling pipe without accounting for the interaction between the pack and the heat exchange system, considers the dynamic interplay between the battery pack and the heat exchange process.

- While conventional studies like [10] often view the battery pack as a singular entity, this study disaggregates it into cells and modules, enhancing the model's accuracy and allowing a more precise representation of thermal phenomena.

The subsequent sections of this article are organized as follows: In Section 2, the thermal model is introduced. Subsequently, in Section 3, the derivation of thermal power is discussed. In Section 4, the thermal model is partially verified using Ansys Transient Thermal Simulation. Detailed simulation results for additional modules of the pack, utilizing a pulse signal as input, are presented in Section 5. Finally, Section 6 discusses the conclusions drawn and outlines paths for future research.

2. THERMAL MODEL

This section delves into comprehending the thermal behavior of a battery pack by initially assessing the heat generated in each cell. The evaluation then extends to encompass each module, taking into account the number of cells within. Subsequently, the total heat generated across the entire pack is determined through the cascaded system. By following this approach, the temperature within the pack can be accurately measured.

2.1 Battery pack

Battery packs consist of groups of battery modules, each containing several lithium-ion batteries arranged in series, parallel, or a combination of both. Between these module units, a heat exchange system is implemented to effectively dissipate heat generated by each individual module unit. The design of the battery pack depicted in Figure 1 draws inspiration from the Tesla Model S Battery Pack.

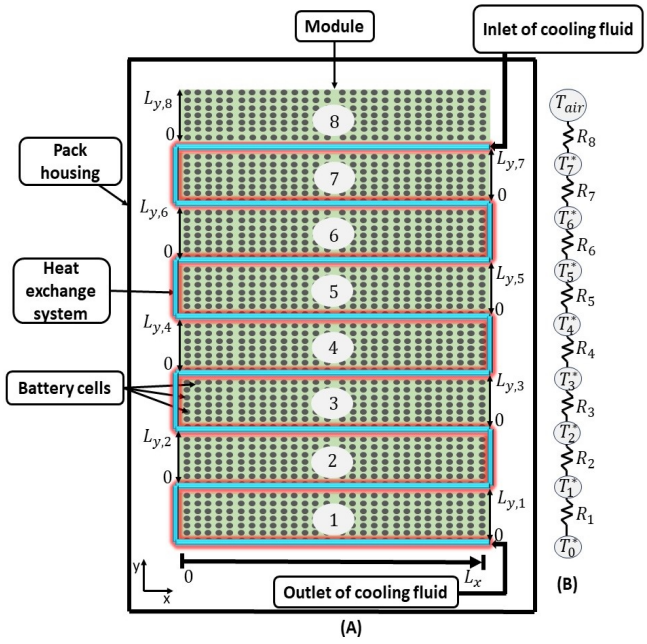

FIGURE 1: (A) SCHEMATIC REPRESENTATION OF BATTERY PACK. (B) THERMAL MODEL DEPICTING THE UTILIZATION OF THERMAL RESISTANCES FOR HEAT TRANSFER ANALYSIS.

2.2 Battery modules

This study employs the heat equation to analyze the thermal distribution within each module unit and, consequently, throughout the battery pack. Equation 1 represents the transient heat equation for each module unit presented in Figure 1 for $i = \overline{1,8}$:

$$\frac{\partial T_i}{\partial t}(t,x,y) = \alpha\left(\frac{\partial^2 T_i(t,x,y)}{\partial x^2} + \frac{\partial^2 T_i(t,x,y)}{\partial y^2}\right) + Q_{\text{module}}(t,x,y),$$
$$\forall (t,x,y) \in (0,\infty)\times(0,L_x)\times(0,L_{y,i}), \quad (1)$$

where α denotes the thermal diffusivity. The boundary conditions will be presented in Section 2.2.3. The internally generated heat within the battery module, Q_{module}, will be presented in Section 2.2.4.

Remark 1 *In a cylindrical cell the axial heat transfer resistance in a spirally wound configuration is notably lower than in the radial direction, leading to a simplified thermal dynamics model that primarily considers radial heat transfer [11]. This explains why the heat exchange system is implemented in the radial direction between two modules.*

2.2.1 The steady-state temperatures at specific points along the interface of the heat exchange system and each module unit, for $i = \overline{1,7}$. The module units are in contact with the heat exchange system, as illustrated in Figure (1), which utilizes water and glycol as a cooling fluid. Consequently, the heat exchange system establishes the boundary conditions for each module. Building on this setup, the first step is to determine the temperatures T_i^* for $i = \overline{0,7}$, as depicted in Figure 1 (B). To calculate these temperatures, a combination of the thermal resistance method and Newton's cooling law was applied. This systematic approach ensures a comprehensive understanding of the thermal dynamics within the module units and their interaction with the heat exchange system.

In Figure 1, each module unit in the y-direction has its own dimension. The design involves the conclusion of one module unit, followed by a heat exchange, and then the commencement of a new module. This design choice results in each module's direction in the y-axis starting from 0 and extending to $L_{y,i}$, the subscript "i" designates the module unit under analysis $i = \overline{1,8}$. Consequently, the frequent occurrence of zeros in the y-direction is a direct outcome of this structural configuration.

Assumption 1 *Considering the heat exchange occurring between two different module units, and assuming that each module unit has an equal number of cells, it is presumed that the heat generated in each module unit at this stage is identical. Consequently, the heat exchange system maintains uniform temperature on both sides. All parameters marked with * are in the steady-state.*

Within the heat exchange system, the role of the working fluid is to dissipate heat and ensure the battery pack remains at a safe temperature. The heat removal within the heat exchange system for each modules is determined using Newton's law of cooling, as expressed in Equation (2), for $i = \overline{1,7}$:

$$q^*_{\text{conv,ex},i} = h_{\text{conv,ex}} A_{\text{conv,ex}} (T_i^* - T^*_{\text{fluid}}), \tag{2}$$

where $h_{\text{conv,ex}}$ represents the local convection heat transfer coefficient, $A_{\text{conv,ex}}$ denotes the internal area of the heat exchange system, T_i signifies the temperature of each module in contact with the heat exchange system wall, and T_{fluid} indicates the temperature of the working fluid.

The conductive heat within each module is calculated using classical thermal resistance methods, where Equation (3) is employed to express conductive heat as $q^*_{\text{cond,ex},i}$. This equation is dependent on the temperature difference between the top part of each module and the bottom temperature of each module in contact with the heat exchange system, divided by the thermal resistance of conduction, denoted as R_i, for $i = \overline{1,7}$.

$$q^*_{\text{cond,ex},i} = \frac{T_i^* - T_{i-1}^*}{R_i}. \tag{3}$$

Assumption 2 *According to the law of conservation of energy, energy cannot be created or destroyed, only transformed. Operating under this premise and assuming no net accumulation of thermal energy within the system (battery module + heat exchange system), the heat conducted out of the module through conduction must equal the heat removed by the heat exchange system via convection. This implies that the heat conducted by the module is effectively dissipated and removed by the heat exchange system through convection.*

Remark 2 *Module 8 is exclusively in contact with the heat exchange system at the bottom, while its left, right, and top sides are exposed to air. Assuming that the temperature at the bottom of module 8, in contact with the heat exchange system, is the same as the top of module 7 in contact with the heat exchange, then for the bottom of module 7, the temperature will be the same as that of the top of module 6, and so on, as shown in Figure 2.*

Applying Assumption 2 and equations (2) and (3), T_7 is derived as:

$$h_{\text{conv,ex}} A_{\text{conv,ex}} (T_7^* - T^*_{\text{fluid}}) = \frac{T_7^* - T_6^*}{R_7},$$
$$T_7^* = \frac{A_{\text{conv,ex}} h_{\text{conv,ex}} R_7 T_{\text{fluid}}(t) - T_6^*}{A_{\text{conv,ex}} h_{\text{conv,ex}} R_7 - 1}.$$

By employing the same logic for each module, the equation for each temperature will be the same with different coefficients. Consequently, here the temperature for each point, for $i = \overline{1,7}$:

$$T_i^* = \frac{A_{\text{conv,ex}} h_{\text{conv,ex}} T_{\text{fluid}} R_i - T_{i-1}^*}{A_{\text{conv,ex}} h_{\text{conv,ex}} R_i - 1}. \tag{4}$$

As the cooling fluid passes through the heat exchange system, the temperature of the surface changes in both the x and y directions. The temperatures T_i^*, for $i = \overline{1,7}$, represent specific points. The calculation of T_i^* begins from T_1 and extends to T_7, with $T_0^* = T_{\text{air}}$. The next step involves determining the boundary conditions for each module, taking into account how the cooling fluid dissipates heat.

Assumption 3 *To the best of the authors' knowledge, precise information about the geometry of the "heat pipe" within the heat exchange system is unavailable. Specifics about the geometry, such as whether the "heat pipe" is cylindrical, oval, or possesses a more square-shaped body, are not provided. Because the length is too long, the "heat pipe" was simplified to a 2D-line to determine the temperature distribution in the x and y directions within the heat exchanger. In Figure 2, the "heat pipe" is where the fluid operates.*

Remark 3 *The classical thermal resistance method was employed to calculate the conductive heat within each module, acknowledging its traditional applicability to 1D steady-state heat transfer without heat generation. In the specific case of a battery module, each cell introduces a heat generation region, and the*

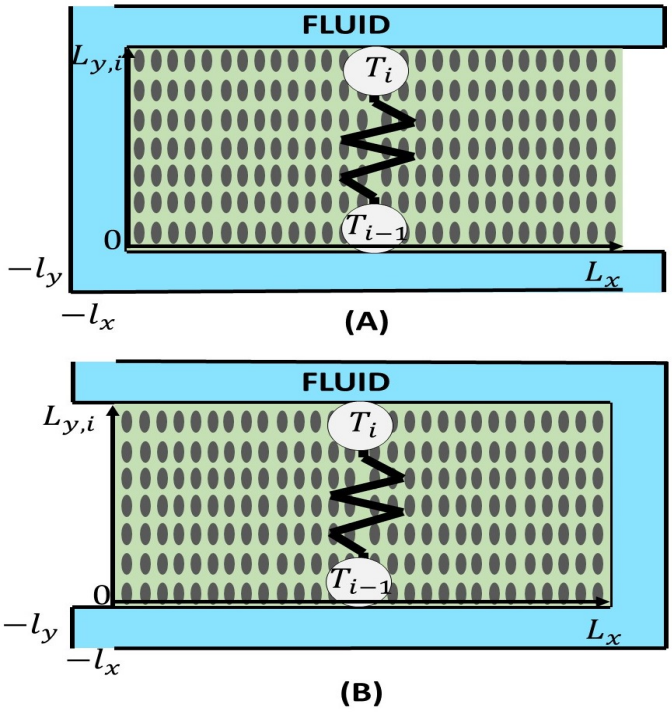

FIGURE 2: MODULE INTERACTION WITH THE HEAT EXCHANGE SYSTEM TO CREATE BOUNDARY CONDITIONS. IN SUB-FIGURE A, $i = 7, 5, 3, 1$, AND IN SUB-FIGURE B, $i = 6, 4, 2$.

overall system may not strictly adhere to a steady state, given that cell-level heat generation is influenced by factors such as current discharge, State-of-Charge (SoC), and local temperature.

To address this deviation from traditional assumptions, our approach involves determining the boundary temperatures of a module by solving the transient energy equation and explicitly accounting for heat generation. This ensures the overall calculations remain physically consistent within the context of a battery module. The net effect of heat generation and transience is captured in the form of boundary temperatures, providing a comprehensive understanding of the thermal behavior.

Remark 4 *In Figure 2, each module unit extends from 0 to L_x in the x-direction, and in the y-direction, each module starts from 0 and extends to $L_{y,i}$. To establish boundary conditions for each module, an analysis should be conducted at the wall of the heat exchange system. For all module units, when x is L_x or y is $L_{y,i}$, the temperature is set to the module temperature T_i. However, it's important to note that L_x and $L_{y,i}$ represent the parts of the module in direct contact with the heat exchange system. Conversely, the parts labeled $-l_x$ and $-l_y$ in Figure 2 are width lengths inside the heat exchange system that do not make contact with each module units. At these points, the temperature is set to T_{fluid}.*

2.2.2 Temperature distribution in the heat exchange system in x and y directions, for $i = \overline{1,7}$. The heat equation, considering uniform energy generation per unit volume, and the temperatures T_i and T_{fluid} in the x direction (as shown in Figure 2), is given by:

$$\frac{\partial^2 T_i(t,x,L_{y,i})}{\partial x^2} + \frac{q^*_{\text{conv,ex},i}}{k} = 0, \quad \forall x \in [-l_x, L_x], \tag{5}$$

with the following boundary conditions:

$$T_i(t, L_x, y) = T_i^*,$$
$$T_i(t, -l_x, y) = T_{\text{fluid}}.$$

The solution of Equation (5) is given by:

$$T_i(t,x,L_{y,i}) = T_{\text{fluid}} + \frac{q^*_{\text{conv,ex},i}}{2k}(l_x^2 - x^2) + \left(T_i^* - T_{\text{fluid}} - \frac{q^*_{\text{conv,ex},i}(l_x^2 - L_x^2)}{2k}\right)\left(\frac{l_x + x}{l_x + L_x}\right), \tag{6}$$

where L_x represents the length in the x-direction as shown in Figure 2, and $q^*_{\text{conv},i}$ is shown in Equation (2), for $i = \overline{1,7}$.

In the y direction, the heat equation is given by:

$$\frac{\partial^2 T_i(t,Lx,y)}{\partial y^2} + \frac{q^*_{\text{conv,ex},i}}{k} = 0, \quad \forall y \in [-l_y, L_{y,i}], \tag{7}$$

with the following boundary conditions:

$$T_i(t, x, L_y) = T_i^*,$$
$$T_i(t, x, -l_y) = T_{\text{fluid}},$$

The solution of Equation (7) is:

$$T_i(t,Lx,y) = T_{\text{fluid}} + \frac{q^*_{\text{conv,ex},i}}{2k}(l_y^2 - y^2) + \left(T_i^* - T_{\text{fluid}} - \frac{q^*_{\text{conv,ex},i}(l_y^2 - L_y^2)}{2k}\right)\left(\frac{l_y + y}{l_y + L_y}\right), \tag{8}$$

where L_y represents the length in the y-direction as shown in Figure 2, for $i = \overline{1,7}$.

The values of T_i^* are obtained from 2.2.1. Each of the PDEs in 2.2.2 are independent and can be solved separately.

2.2.3 Boundary Conditions for each module unit, for $i = \overline{1,8}$. To define the boundaries conditions for each module unit the first step is substitute the temperature from (4) into (6) and (8), it becomes feasible to establish the boundary conditions for (1).

According to Remark 2, the boundary conditions for module 8 are expressed as:

$$T_8(t,x,L_{y,8}) = T_{\text{air}}, \quad \forall (t,x) \in (0,\infty) \times [0, L_x],$$
$$T_8(t,x,0) = T_{\text{fluid}} + \frac{q_{\text{conv,ex},i}}{2k}(l_x^2 - x^2) + \left(\frac{T_7^*}{(l_x + L_x)} - \frac{T_{\text{fluid}}}{(l_x + L_x)} - \frac{q(l_x^2 - L_x^2)}{2k(l_x + L_x)}\right)(l_x + x),$$
$$\forall (t,x) \in (0,\infty) \times [0, L_x],$$
$$T_8(t,0,y) = T_{\text{air}}, \quad \forall (t,y) \in (0,\infty) \times [0, L_{y,8}],$$
$$T_8(t,L_x,y) = T_{\text{air}}, \quad \forall (t,y) \in (0,\infty) \times [0, L_{y,8}].$$

For odd-numbered modules $i = 7, 5, 3, 1$, where contact with ambient air occurs solely on the right side, the boundary conditions are as follows:

$$T_i(t, x, L_{y,i}) = T_{\text{fluid}} + \frac{q_{\text{conv,ex},i}}{2k}(l_x^2 - x^2) + \left(\frac{T_i^*}{(l_x + L_x)} - \frac{T_{\text{fluid}}}{(l_x + L_x)} - \frac{q(l_x^2 - L_x^2)}{2k(l_x + L_x)}\right)(l_x + x), \quad \forall (t, x) \in (0, \infty) \times [0, L_x],$$

$$T_i(t, x, 0) = T_{\text{fluid}} + \frac{q_{\text{conv,ex},i}}{2k}(l_x^2 - x^2) + \left(\frac{T_{i-1}^*}{(l_x + L_x)} - \frac{T_{\text{fluid}}}{(l_x + L_x)} - \frac{q(l_x^2 - L_x^2)}{2k(l_x + L_x)}\right)(l_x + x), \quad \forall (t, x) \in (0, \infty) \times [0, L_x],$$

$$T_i(t, 0, y) = T_{\text{fluid}} + \frac{q_{\text{conv,ex},i}}{2k}(l_y^2 - y^2) + \left(\frac{T_i^*}{(l_y + L_{y,i})} - \frac{T_{\text{fluid}}}{(l_y + L_{y,i})} - \frac{q(l_y^2 - L_{y,i}^2)}{2k(l_y + L_{y,i})}\right)(l_y + y), \quad \forall (t, y) \in (0, \infty) \times [0, L_{y,i}],$$

$$T_i(t, L_x, y) = T_{\text{air}}, \quad \forall (t, y) \in (0, \infty) \times [0, L_{y,i}].$$

For even-numbered modules $i = 6, 4, 2$, where contact with ambient air is present only on the left side, the boundary conditions are as follows:

$$T_i(t, x, L_{y,i}) = T_{\text{fluid}} + \frac{q_{\text{conv,ex},i}}{2k}(l_x^2 - x^2) + \left(\frac{T_i^*}{(l_x + L_x)} - \frac{T_{\text{fluid}}}{(l_x + L_x)} - \frac{q(l_x^2 - L_x^2)}{2k(l_x + L_x)}\right)(l_x + x), \quad \forall (t, x) \in (0, \infty) \times [0, L_x],$$

$$T_i(t, x, 0) = T_{\text{fluid}} + \frac{q_{\text{conv,ex},i}}{2k}(l_x^2 - x^2) + \left(\frac{T_{i-1}^*}{(l_x + L_x)} - \frac{T_{\text{fluid}}}{(l_x + L_x)} - \frac{q(l_x^2 - L_x^2)}{2k(l_x + L_x)}\right)(l_x + x), \quad \forall (t, x) \in (0, \infty) \times [0, L_x],$$

$$T_i(t, 0, y) = T_{\text{air}}, \quad \forall (t, y) \in (0, \infty) \times [0, L_{y,i}],$$

$$T_i(t, L_x, y) = T_{\text{fluid}} + \frac{q_{\text{conv,ex},i}}{2k}(l_x^2 - y^2) + \left(\frac{T_i^*}{(l_y + L_{y,i})} - \frac{T_{\text{fluid}}}{(l_x + L_{y,i})} - \frac{q(l_y^2 - L_{y,i}^2)}{2k(l_y + L_{y,i})}\right)(l_y + x), \quad \forall (t, y) \in (0, \infty) \times [0, L_{y,i}].$$

Since fluid dynamics were not considered, the 8 PDEs are independent of each other. In future work, the dynamics of the working fluid will be taken into account, and the PDEs should be solved from module 8 to 1 in reverse numerical order.

2.2.4 Heat generated in each module unit. With the boundary conditions set for each module, the heat generated Q_{module} within each module is the sum total of heat generated in each cell within the module, described by:

$$Q_{\text{module}}(t) = \frac{\sum Q_{\text{cell}}(t)}{v_{\text{module}}},$$

where $Q_{\text{cell}}(t)$ is the heat generated in each cell, v_{module} is the volume of the module.

2.3 Lithium-ion cell

Within each cylindrical cell, heat is additionally generated due to electrochemical reactions and the contact between various internal components.

Remark 5 *In this study, the generated heat $Q_{cell}(t)$ is divided into three components: one for electrochemical reactions $S_{cell}(t)$, another for the conduction interaction between the components $q^*_{cond,cell}$, and the last one pertains to convective heat transfer of the electrolyte, which is represented as $q^*_{conv,cell}$.*

The heat generated in each cell is described as:

$$Q_{\text{cell}}(t) = S_{\text{cell}}(t) + q^*_{\text{cond,cell}} + q^*_{\text{conv,cell}}.$$

Since $S(t)$ is produced as a function of chemical reactions, it will be discussed in Section 3.

As materials are arranged in a spiral within the cell, interactions occur between the internal components, resulting in the generation of heat due to these interactions. The term $q^*_{\text{cond,cell}}$ represents the heat generated due to this conduction, and it is defined as:

$$q^*_{\text{cond,cell}} = \frac{\Delta T^*}{R_{\text{cell}}} = \frac{T^*_{\text{core}} - T^*_{\text{case}}}{R_{\text{cell}}},$$

where T_{core} represents the core temperature, T_{case} represents the temperature of the case and R_{cell} denotes the total thermal resistance of the material in the spiral and can be expressed as:

$$R_{\text{cell}} = \frac{\ln(r_2/r_1)}{2\pi k_s L_{\text{cell}}},$$

where r_1 represents the internal radius of the cell, r_2 represents the external radius of the cell, L_{cell} represents the length of the spiral, and k_s represents the thermal conductivity of the material in the spiral [12, Chapter 3, Section 3.3.1]. The thermal conductivity is determined through the formula [13]:

$$k_s = \frac{\sum L_{\text{cell}}}{\sum \frac{L_{\text{cell}}}{k_{\text{cell}}}},$$

where L_{cell} denotes the length of each internal part of the spiral inside the battery, and k_{cell} represents the thermal conductivity of these internal components.

The convective heat transfer between the electrolyte and the spiral follows Newton's law of cooling, expressed as:

$$q^*_{\text{conv,cell}} = h_{\text{cell}} A_{\text{cell}} (T^*_{\text{e}} - T^*_{\text{spiral}}),$$

where h_{cell} represents the convective heat transfer coefficient of the electrolyte, A_{cell} is the area covered by the electrolyte, T^*_{e} is the electrolyte temperature, and T^*_{spiral} denotes the temperature of the spiral inside the battery. The temperature T_{e} is determined using the model presented in [14], where a thermal model was developed to calculate the temperature within a cylindrical cell.

Remark 6 *In this study, the created model is utilized to calculate the heat generated in each cylindrical cell. To extend this model to prismatic or pouch cells, the internal resistance must be recalculated, taking into account these different cell geometries.*

3. HEAT GENERATED AS DERIVED FROM THE ELECTROCHEMICAL MODEL

In this model, Joule's effects have been taken into account to convert electric power into thermal power. The result of multiplying current and voltage informs us about the number of electrons moving through a system, along with the energy each electron expends as heat, ultimately providing the total heat production [15]. The required heat, denoted as $S(t)$, is determined using the electrochemical model presented in 3.0.1.

$$S(t) = V(t)I(t).$$

Here, $V(t)$ represents the voltage calculated using the electrochemical model, $I(t)$ is the current applied to the battery.

3.0.1 Electrochemical PDE model. The extensively researched Doyle-Fuller-Newman (DFN) model accurately depicts lithium-ion battery phenomena. However, due to its complexity, simpler approaches such as the Single Particle Model (SPM) have been developed. The SPM treats the electrode as a single spherical particle, simplifies lithium-ion diffusion, and assumes constant electrolyte concentrations. This article employs the SPM within its electrochemical model [16].

Lithium-ions move from the negative pole to the positive pole when discharging, and in the opposite direction when charging. The lithium concentration in the solid phase, and therefore the concentration of lithium-ions in the active material, follows Fick's law of diffusion [16]:

$$\begin{aligned}
&\frac{\partial c_s^{\pm}}{\partial t}(t, r_s) = \frac{1}{r_s^2}\frac{\partial}{\partial r_s}\left[D_s^{\pm}(T(t))r_s^2\frac{\partial c_s^{\pm}}{\partial r_s}(t, r_s)\right], \\
&\qquad t > 0, \quad r_s \in (0, R_s^{\pm}), \\
&\frac{\partial c_s^{\pm}}{\partial r_s}(t, 0) = 0, \quad t > 0, \\
&\frac{\partial c_s^{\pm}}{\partial r_s}(t, R_s^{\pm}) = -\frac{1}{D_s^{\pm}(T(t))}j^{\pm}(t), \quad t > 0, \\
&c_s^{\pm}(0, r_s) = c_{s,0}^{\pm}(r_s), \quad r_s \in [0, R_s^{\pm}],
\end{aligned}$$

where the temporal variable is t, the spatial variable is r_s. The solid phase $c_s^{\pm} \in \mathbb{R}$. $D_s^{\pm}$ is the diffusion of the solid phase. The $j^{\pm}$ is the molar flux given by:

$$j^{+}(t) = -\frac{I(t)}{a_s^{+}FL^{+}}, \quad j^{-}(t) = \frac{I(t)}{a_s^{-}FL^{-}},$$

where $I(t)$ represents the current, $a_s^{\pm}$ stands for the interfacial surface area, F denotes the Faraday constant, and $L^{\pm}$ corresponds to the length of the positive or negative electrode.

Assumption 4 *The diffusion coefficient $D_s^{\pm}$ is a function with Arrhenius-like dependence, inherently influenced by temperature [17], as follows:*

$$D_s^{\pm}(T(t)) = D_s^{\pm}(T(0))e^{E_{D_s^{\pm}}\frac{T(t)-T(0)}{T(t)T(0)}}.$$

$E_{D_s^{\pm}}$ represents the activation energy coefficient, $T(t)$ is the battery temperature. In this article, the diffusion coefficient is considered constant.

The voltage is the difference between the solid electric potentials at the positive and negative electrodes, given by:

$$V(t) = \phi_s^{+}(t) - \phi_s^{-}(t),$$

where the solid electric potentials are given as follows:

$$\phi_s^{\pm}(t) = \eta^{\pm}(t) + U^{\pm}\left(c_{ss}^{\pm}(t), T(t)\right) + FR_f^{\pm}(T(t))j^{\pm}(t).$$

In this context, $\eta^{\pm}(t)$ represents the overpotential, $U^{\pm}\left(c_{ss}^{\pm}(t), T(t)\right)$ is the equilibrium potential, specific to the battery in question and discussed in the simulation results section, F denotes the Faraday constant, and $R_f^{\pm}(T(t))$ signifies the resistance.

The reaction overpotential $\eta^{\pm}$ is defined as:

$$\eta^{\pm}(t) = \frac{RT(t)}{\alpha F}\sinh^{-1}\left(\frac{F}{2i_0^{\pm}(t)}j^{\pm}(t)\right),$$

where R represents the gas constant, T denotes the temperature, α signifies the transfer coefficient, and $i_0^{\pm}$ is expressed as [18]:

$$i_0^{\pm}(t) = k^{\pm}\left[c_{ss}^{\pm}(t)\right]^{\alpha_c}\left[c_{e,0}\left(c_s^{\pm,\max} - c_{ss}^{\pm}(t)\right)\right]^{\alpha_a},$$

where $k^{\pm}$ is the kinetic reaction rate $c_{ss}^{\pm} \triangleq c_s^{\pm}$ represents the boundary concentration in the positive and negative electrodes, and $c_{e,0}$ is the equilibrium electrolyte concentration.

4. THERMAL MODELING VERIFICATION

The thermal model discussed in Section 2 was implemented in MATLAB and verified by comparing it with an ANSYS Transient Thermal simulation. In the ANSYS simulation, the battery module was represented using a 3D geometry (x, y, z). The simulation's maximum time was set to 20,000 seconds to ensure stability. Mesh quality was assessed using Skewness, measured at an excellent value of 1.3×10^{-10}, as referenced in [19]. Figure 3 shows the 3D model in ANSYS with the mesh.

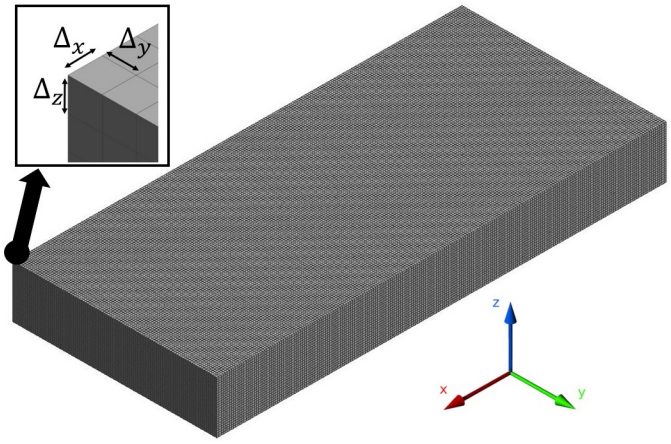

FIGURE 3: THE MESH FOR MODULE 7 IN THE ANSYS TRANSIENT THERMAL ANALYSIS.

Internal heat generation was specified as a constant $39987, \mathrm{W/m^3}$. The temperatures of the heat exchange system were set to 20°C on the top, left, and bottom, while the right

side was set to 23°C. Heat removed from the heat exchange system was −33.27, W on the top and bottom and −15.11, W on the left side. This heat calculation was determined using Equation (2), with the negative sign indicating heat removal by the heat exchange system. Surface conditions were applied to simulate convective heat caused by the air on the surface.

In MATLAB, the boundary conditions, materials, and spatial steps mirrored those used in the ANSYS simulation, as shown in Table 1.

Parameters	ANSYS	MATLAB
Dimensions	3D	2D
Δx	0.0031	0.0031
Δy	0.0031	0.0031
Δz	0.0031	-
Δt	Selected by the Program	0.59 s
Final time	20000	20000
Density	7914	7914
Thermal conductivity	14	14
Heat capacity	1930	1930
Heat Generated	39987	39987
Minimal temperature	22.49°C	20.5°C
Maximum temperature	49.92°C	50.80°C

TABLE 1: COMPARISON OF PARAMETERS BETWEEN ANSYS AND MATLAB.

This verification process focused on a specific module, namely Module 7. Figure 4 illustrates the comparison between the results obtained from ANSYS and those generated by the MATLAB code. Both simulations depict similar shapes, with heat primarily generated in the center of the pack, and the module loses heat at the boundaries due to the heat exchange system. The maximum temperature in both simulations was observed near the center. In the ANSYS simulation, the maximum temperature reached approximately 49.92°C, while in the MATLAB simulation, it was 50.80°C. This analysis suggests that the thermal model presented in this study is effective, providing a reliable representation of temperature for each module.

5. SIMULATION RESULTS

The simulation was performed using MATLAB on a PC from Samsung equipped with an Intel i5-10210U 1.6 GHz CPU and 31.8 GB of RAM. In this study, the modules units were treated as a single unit, resulting in a total of 8 modules units with 888 cells. For the analysis, $LiFePO_4$ 26650 cells were selected, each featuring a voltage of 3.3V and a capacity of 2560 mAh. This specific cell was chosen due to the availability of comprehensive electrochemical parameters in the literature. The equilibrium potential of the active materials in the positive and negative electrodes is denoted as U^+ and U^-, respectively. For the $LiFePO_4$ 26650 battery, the equilibrium potential expressions for the positive and negative electrodes are given as follows [13]:

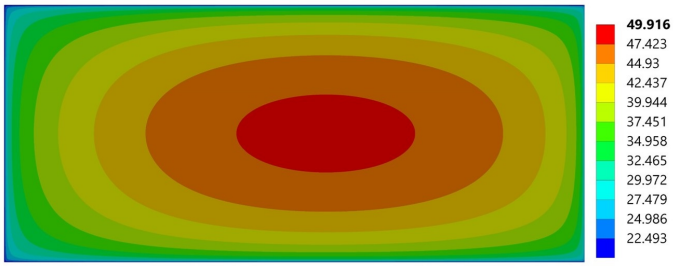

(A) Ansys Simulation

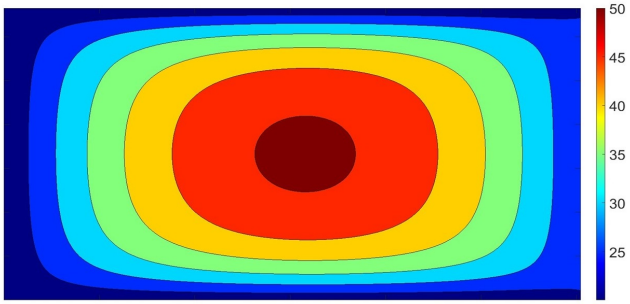

(B) Matlab Simulation

FIGURE 4: VERIFICATION: COMPARISON BETWEEN ANSYS SIMULATION AND MATLAB SIMULATION.

$$
\begin{aligned}
U^+(\theta^+) &= 0.6379 + 0.5416e^{-305.5309\theta^+} \\
&+ 0.044\tanh\left(-\frac{\theta^+ - 0.1958}{0.1088}\right) - 0.1978\tanh\left(\frac{\theta^+ - 1.0571}{0.0854}\right) \\
&- 0.6875\tanh\left(\frac{\theta^+ - 0.0117}{0.0529}\right) - 0.0175\tanh\left(\frac{\theta^+ - 0.5692}{0.0875}\right), \\
U^-(\theta^-) &= 3.4323 - 0.4828e^{-80.2493(1-\theta^-)^{1.3108}} \\
&- 3.2474\times 10^{-6}e^{20.2645(1-\theta^-)^{3.8003}} \\
&+ 3.2482\times 10^{-6}e^{20.2645(1-\theta^-)^{3.7005}},
\end{aligned}
$$

where θ^+ represents the number of moles of lithium within the olivine structure of the iron phosphate in the positive electrode, and θ^- denotes the number of moles of lithium within the graphite structure of the negative electrode [13]. Table 2 shows the electrochemical parameters used in the simulation.

The air temperature outside the battery was set to 25°C, while the temperature of the working fluid inside the heat exchange system was set to 20°C.

Figure 5 illustrates the current profile in pulse format, representing the electrochemical input. The maximum 1 C-rate and minimum -1 C-rate are within the recommended range of 1.2 C-rate for the $LiFePO_4$ 26650 [20].

Figure 6 presents the simulation outcomes obtained in MATLAB, utilizing the current pulse profile illustrated in Figure 5, as the input for the electrochemical model. In this simulation, heat generation is no longer constant; instead, a new heat value is generated within each module every second. The time step, spatial steps, and the final time were the same as those used in Section 4.

Parameters	Values
R_s^+	3.5×10^{-6}
R_s^-	3.65×10^{-8}
L^-	3.5×10^{-5}
L^+	6.5×10^{-5}
ε^+	0.45
ε^-	0.54
F	964870
$C_{\max}$	31370
a^+	$\frac{3}{R_s^+}\varepsilon^+$
a^-	$\frac{3}{R_s^-}\varepsilon^-$
c_0^+	$0.12 \cdot C_{\max}$
c_0^-	$0.86 \cdot C_{\max}$
D_s^+	5.9×10^{-18}
D_s^-	3.0×10^{-14}

TABLE 2: ELECTROCHEMICAL PARAMETERS [13].

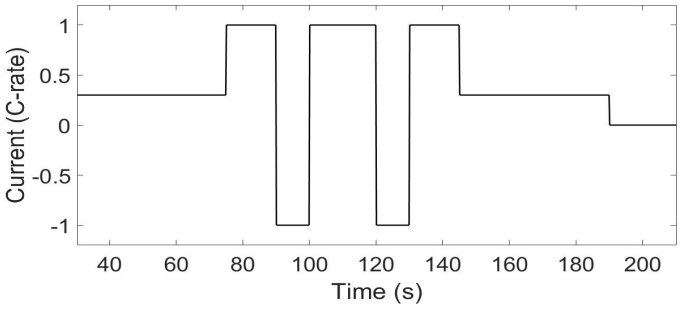

FIGURE 5: CURRENT PROFILE.

Throughout all modules in the pack, the minimum temperature remains approximately 20°C. Notably, Module 8 exhibits the highest temperature peak, reaching around 55°C, in contrast to modules 1 through 7, which have a maximum temperature of 50°C. This variation in the temperature profile in Module 8 can be attributed to the boundary conditions explained in Remark 2. Additionally, heat generation initiates at the center of the modules in all simulations, and heat dissipation occurs through both, the heat exchange system and the air in contact with each module. The variations in temperatures depicted in Figure 6 arise from variations in the current profile, as shown in Figure 5. Changes in the current profile, whether they increase or decrease, affect electrochemical heat generation and subsequently impact temperature behavior.

The odd-numbered modules display nearly identical behavior, characterized by cooler left sides compared to their right sides. In contrast, the even-numbered modules exhibit behavior opposite to that of the odd ones. This behavior corresponds to the positioning of the heat exchange system, which contacts the left side in odd-numbered modules and the right side in even-numbered modules.

Remark 7 *The consistency in temperature profiles across both even and odd modules stems from the assumption of a constant temperature for the working fluid. This assumption is made to simplify the model, presuming that heat removal is uniform across*

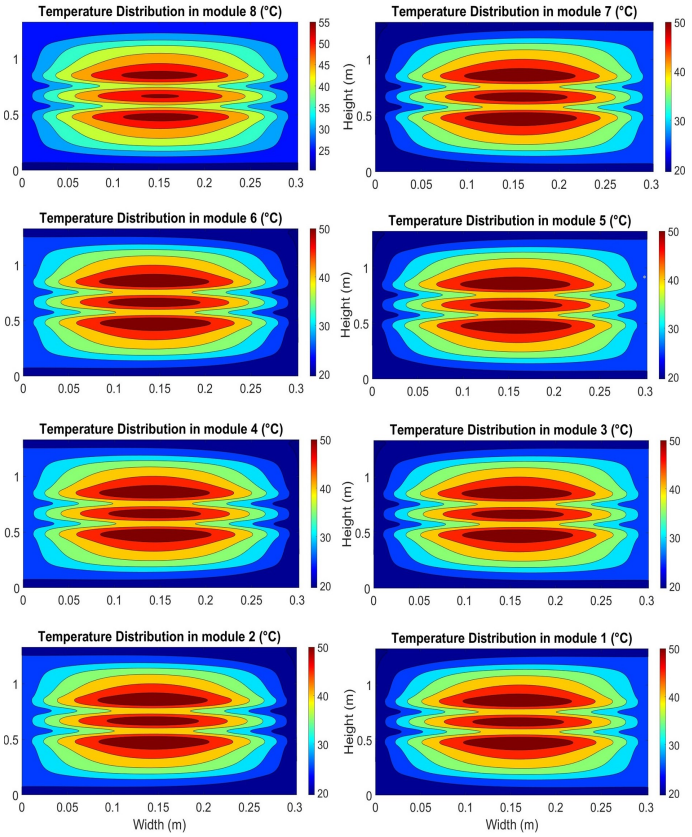

FIGURE 6: PACK SIMULATION: THERMAL SIMULATION OF THE EIGHT MODULES AT 20000 SECONDS.

all modules due to their identical properties such as voltage, current, capacity, volume, and cell count. In future work, these assumptions will be revisited, and a model that accommodates even slight variations in fluid temperature will be developed to ensure an accurate representation of heat absorption in the working fluid. Figure 7 illustrates the temperature difference between modules 7 and 6, with the maximum temperature deviation being $\pm 5°C$.

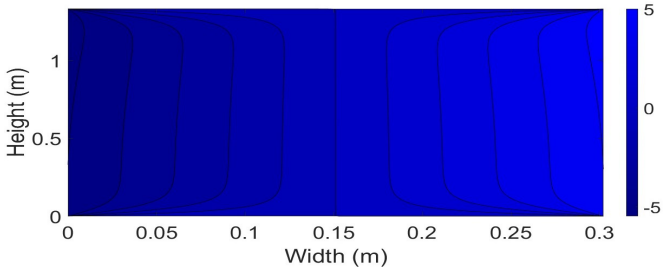

FIGURE 7: TEMPERATURE ERROR BETWEEN MODULE 7 AND 6.

6. CONCLUSION AND FUTURE WORK

This study presents a comprehensive investigation that integrates a thermal and electrochemical model for a lithium-ion battery pack featuring cylindrical cells. The thermal model encompasses three domains, initiating with a focus on a single

cylindrical cell, progressing to a module with cells arranged uniformly, and extending to the battery pack level, comprising multiple modules. This unified model is designed to determine the temperature distribution within battery packs, calculating heat generation in individual cells through an electrochemical model. It incorporates thermal resistances for conduction and considers convection effects. The Finite Difference Method is applied to extrapolate the heat generated in each cell to the module units, thereby determining the temperature in each unit. The thermal model's validity was confirmed through verification using Ansys thermal analysis.

In future work, Assumption 1 will be relaxed, allowing the values of $q^*_{\text{conv,ex},i}$ and $q^*_{\text{cond,ex},i}$ to exhibit dynamic behavior rather than being considered constant, for $i = \overline{1,7}$. The thermal model will play a crucial role as the foundation for developing temperature and electrochemical estimators, thereby facilitating precise monitoring and control of temperature variations within the battery packs.

REFERENCES

[1] Keiner, Dominik, Thoma, Christian, Bogdanov, Dmitrii and Breyer, Christian. "Seasonal hydrogen storage for residential on-and off-grid solar photovoltaics prosumer applications: Revolutionary solution or niche market for the energy transition until 2050?" *Applied Energy* Vol. 340 (2023): p. 121009.

[2] Muratori, Matteo, Alexander, Marcus, Arent, Doug, Bazilian, Morgan, Cazzola, Pierpaolo, Dede, Ercan M, Farrell, John, Gearhart, Chris, Greene, David, Jenn, Alan et al. "The rise of electric vehicles—2020 status and future expectations." *Progress in Energy* Vol. 3 No. 2 (2021): p. 022002.

[3] Galatro, Daniela, Al-Zareer, Maan, Da Silva, Carlos, Romero, David and Amon, Cristina. "Thermal behavior of lithium-ion batteries: Aging, heat generation, thermal management and failure." *Frontiers in Heat and Mass Transfer (FHMT)* Vol. 14.

[4] Nam, Kyung-Wan, Bak, Seong-Min, Hu, Enyuan, Yu, Xiqian, Zhou, Youngning, Wang, Xiaojian, Wu, Lijun, Zhu, Yimei, Chung, Kyung-Yoon and Yang, Xiao-Qing. "Combining in situ synchrotron X-ray diffraction and absorption techniques with transmission electron microscopy to study the origin of thermal instability in overcharged cathode materials for lithium-ion batteries." *Advanced Functional Materials* Vol. 23 No. 8 (2013): pp. 1047–1063.

[5] Song, Liubin, Zheng, Youhang, Xiao, Zhongliang, Wang, Cheng and Long, Tianyuan. "Review on thermal runaway of lithium-ion batteries for electric vehicles." *Journal of Electronic Materials* Vol. 51 No. 1 (2022): pp. 30–46.

[6] Arora, Shashank. "Selection of thermal management system for modular battery packs of electric vehicles: A review of existing and emerging technologies." *Journal of Power Sources* Vol. 400 (2018): pp. 621–640.

[7] Berdichevsky, Gene, Kelty, Kurt, Straubel, JB and Toomre, Erik. "The tesla roadster battery system." *Tesla Motors* Vol. 1 No. 5 (2006): pp. 1–5.

[8] Xie, Yi, Zheng, Jintao, Li, Wei, Lee, Kuining, Zhang, Yangjun, Liu, Jiangyan, Dan, Dan, Wu, Cunxue and Wang, Pingzhong. "An improved electrothermal-coupled model for the temperature estimation of an air-cooled battery pack." *International Journal of Energy Research* Vol. 44 No. 3 (2020): pp. 2037–2060.

[9] Smyshlyaev, Andrey, Krstic, Miroslav, Chaturvedi, Nalin, Ahmed, Jasim and Kojic, Aleksandar. "PDE model for thermal dynamics of a large Li-ion battery pack." *Proceedings of the American Control Conference* DOI 10.1109/ACC.2011.5991584.

[10] Tian, Ning, Fang, Huazhen and Wang, Yebin. "3-D temperature field reconstruction for a lithium-ion battery pack: A distributed Kalman filtering approach." *IEEE Transactions on Control Systems Technology* Vol. 27 No. 2 (2017): pp. 847–854.

[11] Zhang, Dong, Dey, Satadru, Tang, Shu-Xia, Drummond, Ross and Moura, Scott J. "Battery internal temperature estimation via a semilinear thermal PDE model." *Automatica* Vol. 133 (2021): p. 109849.

[12] Bergman, Theodore L, Lavine, Adrienne S, Incropera, Frank P and DeWitt, David P. *Introduction to heat transfer*. John Wiley & Sons (2011).

[13] Chiew, J., Chin, C. S., Toh, W. D., Gao, Z., Jia, J. and Zhang, C. Z. "A pseudo three-dimensional electrochemical-thermal model of a cylindrical $LiFePO_4$-graphite battery." *Applied Thermal Engineering* Vol. 147 (2019): pp. 450–463.

[14] Ferreira, Patryck and Tang, Shu-Xia. "Sensors Placement Analysis and Temperature Estimation in Lithium-Ion Batteries with a Cascaded Electrochemical-Thermal Model." *European Control Conference (ECC, 2024)* .

[15] Von Meier, Alexandra. *Electric power systems: a conceptual introduction*. John Wiley & Sons (2006).

[16] Chaturvedi, Nalin A, Klein, Reinhardt, Christensen, Jake, Ahmed, Jasim and Kojic, Aleksandar. "Algorithms for advanced battery-management systems." *IEEE Control systems magazine* Vol. 30 No. 3 (2010): pp. 49–68.

[17] Klein, Reinhardt, Chaturvedi, Nalin A, Christensen, Jake, Ahmed, Jasim, Findeisen, Rolf and Kojic, Aleksandar. "Electrochemical model based observer design for a lithium-ion battery." *IEEE Transactions on Control Systems Technology* Vol. 21 No. 2 (2012): pp. 289–301.

[18] Moura, Scott J, Argomedo, Federico Bribiesca, Klein, Reinhardt, Mirtabatabaei, Anahita and Krstic, Miroslav. "Battery state estimation for a single particle model with electrolyte dynamics." *IEEE Transactions on Control Systems Technology* Vol. 25 No. 2 (2016): pp. 453–468.

[19] FEATips. "Mesh Quality and Advanced Topics." (2021). Accessed data de acesso, URL https://featips.com/wp-content/uploads/2021/05/Mesh-Intro_16.0_L07_Mesh_Quality_and_Advanced_Topics.pdf.

[20] Inc., Lithium Werks. "Lithium Werks' 26650 Ion Power Cell." https://lithiumwerks.com/products/lithium-ion-26650-cells/ (2021). Lithium Werks' 26650 cells are best for Power.Safety.Life.™ applications. Copyright © 2021 Lithium Werks Inc.